ATLAS NOTE

ATLAS-CONF-2012-036

March 11, 2012

Search for Scalar Top Quark Pair Production in Natural Gauge Mediated Supersymmetry Models with the ATLAS Detector in pp Collisions at $\sqrt{s} = 7$ TeV

ATLAS Collaboration

Abstract

The results of a search for pair production of the lighter scalar partners of top quarks ($\tilde{t}_1$) in 2.05 fb^{-1} of pp collisions at $\sqrt{s} = 7$ TeV using the ATLAS experiment are reported. Scalar top quarks are searched for in events with two same flavour opposite-sign leptons (e, μ) with invariant mass consistent with the Z boson mass, large missing transverse momentum and jets in the final state. At least one of the jets is identified as originating from a b-quark. No excess over Standard Model expectations is found. The results are interpreted in the framework of R-parity conserving, gauge-mediated Supersymmetry breaking 'natural' scenarios where the neutralino ($\tilde{\chi}_1^0$) is the next-to-lightest supersymmetric particle. Scalar top quark masses up to 310 GeV are excluded for 115 GeV $< m_{\tilde{\chi}_1^0} <$ 230 GeV at 95% confidence-level, reaching an exclusion of $m_{\tilde{t}_1} <$ 330 GeV for $m_{\tilde{\chi}_1^0} = 190$ GeV.

1 Introduction

Supersymmetry (SUSY) [1–9] provides an extension to the Standard Model (SM) which can naturally resolve the hierarchy problem. For each known boson or fermion, SUSY introduces a particle (sparticle) with identical quantum numbers except for a difference of half a unit of spin. The non-observation of the sparticles implies that SUSY is broken and the superpartners are generally heavier than the SM partners. In the framework of a generic R-parity conserving minimal supersymmetric extension of the SM (MSSM) [10–14], SUSY particles are produced in pairs and the lightest supersymmetric particle (LSP) is stable.

The scalar partners of right-handed and left-handed quarks, $\tilde{q}_R$ and $\tilde{q}_L$, can mix to form two mass eigenstates. In the case of the scalar top quark ($\tilde{t}$, stop), large mixing effects due to the Yukawa coupling, y_t, and the trilinear coupling, A_t, can lead to one stop mass eigenstate, $\tilde{t}_1$, that is significantly lighter than other squarks. Consequently, $\tilde{t}_1$ could be produced with large cross sections at the LHC via direct pair production.

Light stop masses are favoured by arguments of 'naturalness' of the electroweak symmetry breaking [15], because of the possibly large coupling between the $\tilde{t}$ and the Higgs boson, h. In particular, radiative corrections to the Higgs boson mass mainly arise from the stop-top loop diagrams including top Yukawa and three-point stop-stop-Higgs interactions.

The conditions for naturalness depend on the SUSY breaking mechanism. In gauge-mediated SUSY breaking (GMSB) models [16,17], gauge interactions (messengers) are responsible for the appearance of soft supersymmetry breaking terms. If the characteristic scale of the masses of the messenger fields is about 10 TeV, an upper bound on $m_{\tilde{t}_1}$ of about 400 GeV is found when imposing the absence of significant ($\sim 10\%$) fine tuning [15].

In GMSB, the gravitino $\tilde{G}$ is the LSP (in general $m_{\tilde{G}} < 1$ keV). The experimental signatures are largely determined by the nature of the next-to-lightest SUSY particle (NLSP). For several GMSB models the NLSP is the lightest neutralino, $\tilde{\chi}_1^0$, promptly decaying to its lighter SM partner through gravitino emission. Neutralinos are mixtures of gaugino ($\tilde{B}$, $\tilde{W}^0$) and higgsino ($\tilde{H}_u^0$, $\tilde{H}_d^0$) gauge-eigenstates, and therefore the lightest neutralino decays to either a γ, Z or Higgs boson. If the $\tilde{\chi}_1^0$ is higgsino-like, it decays either via $\tilde{\chi}_1^0 \to h\tilde{G}$ or $\tilde{\chi}_1^0 \to Z\tilde{G}$. Light higgsinos, also required by naturalness arguments, lead to a large higgsino component in $\tilde{\chi}_1^0$ and a small mass difference between $\tilde{\chi}_1^0$ and $\tilde{\chi}_1^\pm$. In particular, if the higgsino mass $|\mu|$ is much smaller than the gaugino masses (pure higgsino case), $\tilde{\chi}_1^0$ and $\tilde{\chi}_1^\pm$ are almost degenerate such that the (ff') system resulting from the chargino decay $\tilde{\chi}_1^\pm \to \tilde{\chi}_1^0 ff'$ is very soft.

In this letter, a search for direct stop pair production is presented, assuming a GMSB model [18] where the $\tilde{\chi}_1^0$ is purely higgsino-like and is lighter than the $\tilde{t}_1$. The model parameters, fixed to follow naturalness arguments, are

$$m_{\tilde{q}_3} = m_{\tilde{u}_3} = -A_t/2; \quad \tan\beta = 10, \tag{1}$$

where $m_{\tilde{q}_3}$ and $m_{\tilde{u}_3}$ are the soft SUSY breaking masses for the left- and right-handed third-generation squarks, respectively, and $\tan\beta$ is the ratio of the vacuum expectation values of up-type and down-type Higgs field. The $\tilde{t}$ mass eigenstates are such that $m_{\tilde{t}_2} \gg m_{\tilde{t}_1}$ and only $\tilde{t}_1\tilde{t}_1$ pair production is considered in the following. Stops decay either via $\tilde{t}_1 \to b\tilde{\chi}_1^+$ or, if kinematically allowed, via $\tilde{t}_1 \to t\tilde{\chi}_{1(2)}^0$. For the scenarios considered, the subsequent decay $\tilde{\chi}_1^0 \to Z\tilde{G}$ has a branching ratio (BR) between 1 and 0.65 for $m_{\tilde{\chi}_1^0}$ between 100 and 350 GeV. Thus, the expected signal is characterised by the presence of two jets originating from the hadronisation of the b-quarks (b-jets), decay products of Z (or h) bosons and large missing transverse momentum — its magnitude is referred to as $E_{\mathrm{T}}^{\mathrm{miss}}$ in the following — resulting from the undetected

gravitinos.

This search uses data recorded between March and August 2011 at the LHC. After the application of beam, detector, and data quality requirements, the dataset corresponds to a total integrated luminosity of 2.05 ± 0.08 fb^{-1} [19, 20]. To enhance the sensitivity to the aforementioned SUSY scenarios, events are required to contain energetic jets, of which one must be identified as a b-jet, large $E_{\mathrm{T}}^{\mathrm{miss}}$ and two opposite-sign, same flavour leptons ($\ell = e, \mu$) with invariant mass consistent with the Z boson mass, m_Z. This is the first search for this kind of SUSY models.

2 The ATLAS Detector

The ATLAS detector [21] consists of inner tracking devices surrounded by a superconducting solenoid, electromagnetic and hadronic calorimeters and a muon spectrometer with a toroidal magnetic field.

The inner detector system, in combination with the 2 T field from the solenoid, provides precision tracking of charged particles for $|\eta| < 2.5$ [1]. It consists of a silicon pixel detector, a silicon microstrip detector and a straw tube tracker that also provides transition radiation measurements for electron identification. The calorimeter system covers the pseudorapidity range $|\eta| < 4.9$. It is composed of sampling calorimeters with either liquid argon (LAr) or scintillating tiles as the active media. The muon spectrometer surrounds the calorimeters. It consists of a set of high-precision tracking chambers placed within a magnetic field generated by three large superconducting eight-coil toroids. The spectrometer, which has a separate trigger for $|\eta| < 2.4$, provides muon identification and measurement for $|\eta| < 2.7$.

3 Simulated Event Samples

Simulated event samples are used to aid in the description of the background, as well as to determine the detector acceptance, the reconstruction efficiencies and the expected event yields for the SUSY signal.

The signal samples are simulated with the HERWIG++ [22] v2.4.2 Monte Carlo (MC) program at fixed $\tilde{t}_1$ and $\tilde{\chi}_1^0$ masses, obtaining the desired values by varying the $m_{\tilde{q}_3}$ and $|\mu|$ parameters. The particle mass spectra and decay modes are determined using ISASUSY from the ISAJET [23] v7.80 program. The SUSY sample yields are normalised to the results of next-to-leading order (NLO) calculations as obtained using PROSPINO [24] v2.1 including higher order supersymmetric QCD corrections and the resummation of soft gluon emission at next-to-leading-logarithmic (NLL) accuracy [25]. An envelope of cross section predictions is defined using the 68% C.L. ranges of the CTEQ6.6M [26] (including α_s uncertainty) and MSTW2008 [27] PDF sets, together with variations of the factorisation and renormalisation scales, set to the stop mass. The nominal cross section value is taken to be the midpoint of the envelope and the uncertainty assigned is half the full width of the envelope, following closely the PDF4LHC recommendations [28]. NLO+NLL cross sections vary between 80 pb and 0.1 pb for stop masses in the range of 140–450 GeV.

[1] ATLAS uses a right-handed coordinate system with its origin at the nominal interaction point (IP) in the centre of the detector and the z-axis coinciding with the axis of the beam pipe. The x-axis points from the IP to the center of the LHC ring, and the y-axis points upward. Cylindrical coordinates (r, ϕ) are used in the transverse plane, ϕ being the azimuthal angle around the beam pipe. The pseudorapidity is defined in terms of the polar angle θ as $\eta = -\ln\tan(\theta/2)$. The distance ΔR in the $\eta - \phi$ space is defined as $\Delta R = \sqrt{(\Delta\eta)^2 + (\Delta\phi)^2}$.

For the backgrounds the following SM processes are considered. Top quark pair and single top quark production are simulated with MC@NLO [29], setting the top quark mass to 172.5 GeV, and using the NLO PDF set CTEQ6.6 [30]. Additional samples generated with POWHEG [31] and ACERMC [32] are used to estimate the event generator systematic uncertainties. Samples of W+jets, Z/γ^*+jets with light- and heavy-flavour jets, and $t\bar{t}$ with additional b-jets, $t\bar{t}b\bar{b}$, are generated with ALPGEN [33] and the PDF set CTEQ6L1 [34]. The fragmentation and hadronisation for the ALPGEN and MC@NLO samples are performed with HERWIG [35], using JIMMY [36] for the underlying event. Samples of $Zt\bar{t}$ and $Wt\bar{t}$ are generated with MADGRAPH [37] interfaced to PYTHIA [38]. Diboson (WW, WZ, ZZ) samples are generated with HERWIG. For the comparison to data, all SM background cross sections are normalised to the results of higher order calculations [39].

The MC samples are produced using PYTHIA and HERWIG/JIMMY parameters tuned as described in Ref. [40] and are processed through a detector simulation [41] based on GEANT4 [42]. Effects of multiple proton–proton interactions [40] are included in the simulation and MC events are re-weighted to reproduce the mean expected number of collisions per bunch crossing estimated from data.

4 Object reconstruction

Jet candidates are reconstructed using the anti-k_t jet clustering algorithm [43, 44] with a radius parameter of 0.4. The inputs to the algorithm are three-dimensional calorimeter energy clusters [45] seeded by cells with energy calibrated at the electromagnetic scale significantly above the measured noise. The measured jet energy is corrected for inhomogeneities and for the non-compensating nature of the calorimeter by using p_{T}- and η-dependent correction factors derived using simulated multi-jet events (Ref. [46] and references therein). Only jet candidates with $p_{\mathrm{T}} > 20$ GeV and $|\eta| < 2.8$ are retained.

A b-tagging algorithm exploiting both impact parameter and secondary vertex information [47] is used to identify jets containing a b-hadron decay. The algorithm is based on a multivariate technique that uses quantities such as impact parameter of the tracks associated to the secondary vertex, tracks in jet and other jet shape information. The nominal b-tagging efficiency, computed on $t\bar{t}$ MC events, is on average 60%, with a misidentification (mis-tag) rate for light quark/gluon jets of less than 1%. These b-jets are identified within the nominal acceptance of the inner detector ($|\eta| < 2.5$) and are required to have $p_{\mathrm{T}} > 50$ GeV.

Electron candidates are required to have $p_{\mathrm{T}} > 20$ GeV and $|\eta| < 2.47$, and are selected to satisfy the 'tight' shower shape and track selection criteria of Ref. [48]. The candidate electron must be isolated, such that the p_{T} sum of tracks (Σp_{T}, not including the electron track) within a cone in the (η, ϕ) plane of radius $\Delta R = 0.2$ around the candidate must be less than 10% of the electron p_{T}.

Muons are reconstructed using an algorithm [49] which combines the inner detector and the muon spectrometer information (combined muons). A muon is selected for the analysis only if it has $p_{\mathrm{T}} > 10$ GeV and $|\eta| < 2.4$, and the sum of the transverse momenta of tracks within a cone of $\Delta R = 0.2$ around it is less than 1.8 GeV. To reject cosmic rays, muons are required to have longitudinal and transverse impact parameters within 1 mm and 0.2 mm of the primary vertex, respectively.

Following the object reconstruction described above, overlaps between jet candidates and leptons are resolved. Any jet within a distance $\Delta R = 0.2$ of a candidate electron is discarded. Any remaining lepton within $\Delta R = 0.4$ of a jet is discarded.

The $E_{\mathrm{T}}^{\mathrm{miss}}$ is calculated as the sum of terms obtained from the vectorial sum of the transverse

momenta of jets (with $p_{\mathrm{T}} > 20$ GeV and $|\eta| < 4.5$), electrons and muons – including non-isolated muons [50]. The four-vectors of calorimeter clusters not belonging to other reconstructed objects are also added.

During 40% of the data-taking period, a localised electronics failure in the LAr barrel calorimeter created a dead region in the second and third calorimeter layers ($\Delta\eta \times \Delta\phi \simeq 1.4 \times 0.2$) in which, on average, 30% of the incident energy is not measured. If a jet with $p_{\mathrm{T}} > 50$ GeV or an electron candidate falls in this region, the event is rejected. The loss in signal acceptance is below 10% for the models considered.

5 Event Selection

The data are selected with a three-level trigger system based on the presence of leptons. Two trigger paths are considered: a single electron trigger, reaching a plateau efficiency for electrons with $p_{\mathrm{T}} \geq 25$ GeV, and a combined muon+jet trigger, reaching the plateau efficiency for muons with $p_{\mathrm{T}} \geq 20$ GeV and jets with $p_{\mathrm{T}} \geq 60$ GeV.

Events are required to have a reconstructed primary vertex associated with five or more tracks and must pass basic quality criteria against detector noise and non-collision backgrounds [46]. The selections applied in this analysis are listed below.

- To ensure full efficiency of the trigger, events are selected if they contain at least one lepton with $p_{\mathrm{T}} > 25$ GeV for electrons and $p_{\mathrm{T}} > 20$ GeV for muons.
- Exactly two same flavour opposite-sign leptons ($ee, \mu\mu$) are required, such that their invariant mass $m_{\ell\ell}$ is within the Z mass range (86 GeV $< m_{\ell\ell} <$ 96 GeV). Events with additional electron or muon candidates are vetoed.
- Events must include at least one jet with $p_{\mathrm{T}} > 60$ GeV and one additional jet with $p_{\mathrm{T}} >$ 50 GeV.
- At least one jet with $p_{\mathrm{T}} > 50$ GeV and $|\eta| < 2.5$ is required to be b-tagged.

Two signal regions, referred to as SR1 and SR2, are defined using two different $E_{\mathrm{T}}^{\mathrm{miss}}$ threshold requirements in order to maximise the sensitivity across the $\tilde{t}_1$-$\tilde{\chi}_1^0$ mass plane. For SR1, $E_{\mathrm{T}}^{\mathrm{miss}} > 50$ GeV is required and it is optimised for models with $\Delta m = m_{\tilde{t}_1} - m_{\tilde{\chi}_1^0}$ larger than 100 GeV or $m_{\tilde{t}_1} < 300$ GeV, where moderate missing transverse momentum is expected. SR2 is optimised for small Δm scenarios and events are required to have $E_{\mathrm{T}}^{\mathrm{miss}} > 80$ GeV.

The signal efficiencies, including $Z \to ee, \mu\mu$ BR, acceptance and detector effects, vary across the $\tilde{t}_1$-$\tilde{\chi}_1^0$ mass plane. For SR1 (SR2) the efficiencies are found to lie between 0.03% and 2.1% (0.01% and 1.7%) as the stop mass increases from 140 GeV to 400 GeV, and between 0.6% and 2.0% (0.5% and 1.7%) for Δm between 300 and 100 GeV at a stop mass of 400 GeV.

6 Background Estimation

The main SM processes contributing to the background are, in order of importance, top quark pair and single top quark production, followed by the associated production of Z bosons and heavy-flavour jets — referred to as Z+hf.

The top background is evaluated using control regions (CRs) that are the same as the SRs with the exception of the $m_{\ell\ell}$ requirement (modified to 15 GeV $< m_{\ell\ell} <$ 81 GeV, $m_{\ell\ell} >$ 101 GeV). Depending on the corresponding signal region, CRs are labelled as CR1 and CR2. In both cases,

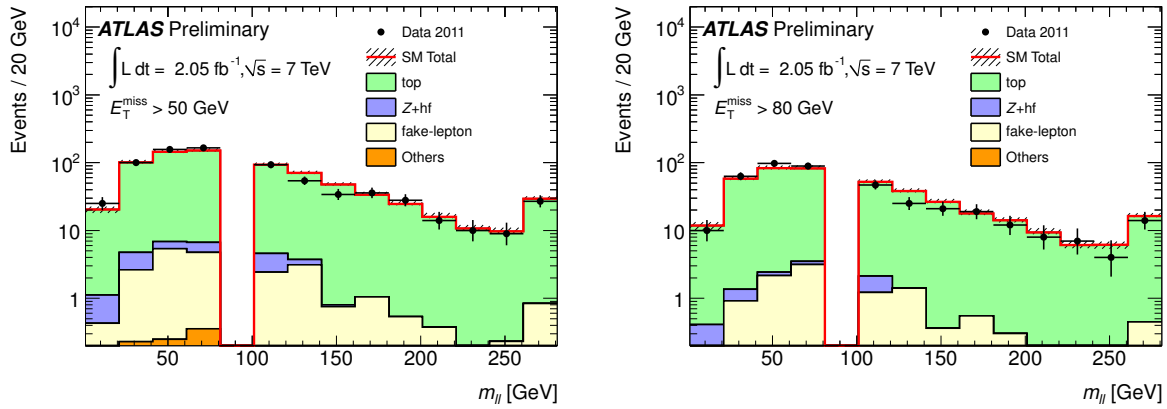

Figure 1: The distribution of $m_{\ell\ell}$ in CR1 (left) and CR2 (right) for the sum of ee and $\mu\mu$ channels. The dashed band shows the experimental systematic uncertainties including effects due to JES, b-tagging and lepton ID efficiency. The last $m_{\ell\ell}$ bin includes the number of overflow events for both data and SM expectation.

low yields from the targeted SUSY signals are expected. The background estimation in each SR is obtained by multiplying the number of events observed in the corresponding CR – corrected using simulations for non-top backgrounds – by a transfer factor, defined as the ratio of the MC predicted yield in the signal region to that in the control region:

$$N_{\mathrm{SR}}^{\mathrm{top}} = \frac{N_{\mathrm{SR}}^{\mathrm{top,MC}}}{N_{\mathrm{CR}}^{\mathrm{top,MC}}} \left(N_{\mathrm{CR}}^{\mathrm{obs}} - N_{\mathrm{CR}}^{\mathrm{non\text{-}top,MC}} \right) \tag{2}$$

where $N_{\mathrm{CR}}^{\mathrm{obs}}$ denotes the observed yield in the CR. For each CR, the contribution from other SM processes accounts for less than 10% of the total. The estimate based on this approach benefits from a cancellation of systematic uncertainties that are correlated between SRs and CRs. The distribution of $m_{\ell\ell}$ for CR1 is shown in Figure 1. Contributions from ee and $\mu\mu$ events are summed. The experimental uncertainties, described in Section 7, are displayed. They include effects due to jet energy scale and resolution [46] (JES), b-tagging [47] and lepton identification (ID) efficiencies [48,49,51]. The number of expected events for 2.05 fb^{-1} of integrated luminosity as predicted by the MC is in good agreement with data for both CRs without introducing data/MC scaling factors.

The topology of Z+hf production events is similar to that of the signal, especially in low $\tilde{t}_1$-$\tilde{\chi}_1^0$ mass scenarios. Therefore the background from the Z+hf process is estimated from MC simulation and validated in a control region where events passing all SR selection criteria except for a reversed $E_{\mathrm{T}}^{\mathrm{miss}}$ cut ($E_{\mathrm{T}}^{\mathrm{miss}} < 50$ GeV) are considered. In Figure 2 the $E_{\mathrm{T}}^{\mathrm{miss}}$ distribution in the range 0–50 GeV is shown for ee+$\mu\mu$ final states. The number of events observed in data is in good agreement with the SM expected yields within experimental uncertainties. Possible signal contamination in this control region varies across the $\tilde{t}_1$-$\tilde{\chi}_1^0$ mass range from 5% to about 50% of the total predicted SM background, with a maximum of 80% for $m_{\tilde{t}_1} \simeq 150$ GeV and $m_{\tilde{\chi}_1^0} \simeq 100$ GeV.

Backgrounds from W+jets and multi-jet production, referred to as "fake-lepton" contributions, are sub-dominant. In this case, events passing the selection contain at least one misidentified (fake) or a non-isolated lepton. The fake-lepton background estimate is obtained using the data-driven approach described in Ref. [52]. The probability of misidentifying a jet as a

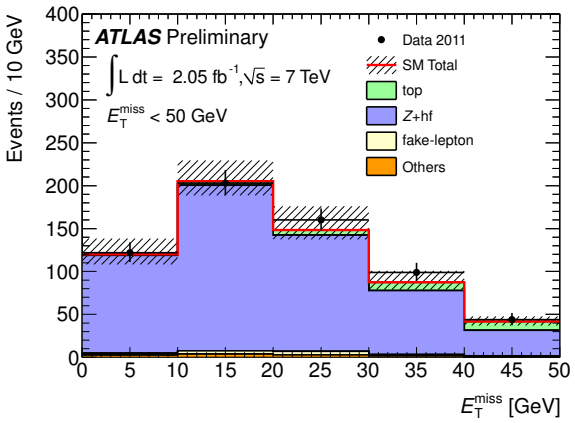

Figure 2: The distribution of $E_{\mathrm{T}}^{\mathrm{miss}}$ for the Z+hf validation region for the sum of ee and $\mu\mu$ channels. By construction, only events with $E_{\mathrm{T}}^{\mathrm{miss}}$ below 50 GeV are displayed. The dashed grey band represents the experimental uncertainties including effects due to JES, b-tagging and lepton ID efficiency.

signal lepton is estimated in control regions dominated by multi-jet events where exactly one pre-selected lepton, at least one b-tagged jet and low $E_{\mathrm{T}}^{\mathrm{miss}}$ are required.

Finally, background contributions from diboson, $Zt\bar{t}$, $Wt\bar{t}$ and $t\bar{t}b\bar{b}$ events are estimated from MC simulation. They account for less than 3% of the total SM background in either SR.

7 Systematic uncertainties

Various systematic uncertainties affecting the background rates and signal yields have been considered.

Systematic uncertainties on the top background expectations vary between 11% and 13% depending on the SR and are dominated by the residual uncertainties on the shape of the top kinematic distributions. The uncertainties are evaluated using additional MC samples generated with ACERMC [32], for the impact of initial and final state radiation parameters varied as in Ref. [53], PYTHIA and POWHEG [31] for choice of fragmentation model and generator, respectively. Experimental uncertainties on the b-tagging efficiency, JES and lepton ID efficiency account for about 4% in either SRs.

The dominant uncertainties on the Z+hf background estimates from simulation arise from the $\pm 55\%$ uncertainty on the production cross section used to normalise the MC yields. The uncertainty is evaluated from the direct Z+hf measurement described in Ref. [54] and takes into account differences between data, MCFM [55] and ALPGEN predictions. The extrapolation of the total production cross section uncertainty to each following jet multiplicity in $Z+N$jets events increases such uncertainty by an additional 24% [56]. Other uncertainties due to JES, b-tagging efficiency and lepton ID efficiency are found to be about 25% and 35% for SR1 and SR2, respectively.

The estimated fake-lepton background is affected by systematic uncertainties related to the determination of the lepton misidentification rate and to the subtraction of non-multi-jet contributions to the event yield in the multi-jet enhanced regions. The estimated uncertainty is 50% and 60% in SR1 and SR2, respectively.

For the SUSY signal processes, uncertainties on the renormalisation and factorisation scales,

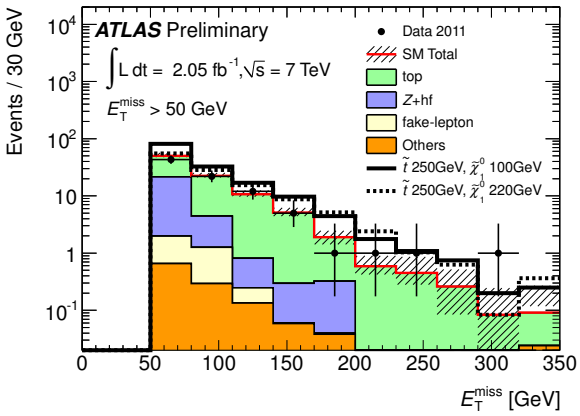

Figure 3: The ee+$\mu\mu$ $E_{\mathrm{T}}^{\mathrm{miss}}$ distribution for SR1 compared to the SM predictions (solid red line) and SM+signal predictions (solid and dashed black lines). The dashed grey band represents the total systematic uncertainties.

on the PDF and on α_s affect the cross section predictions. PDF and α_s uncertainties are between 10% and 15% depending on $m_{\tilde{t}_1}$ for the mass range considered. The variation of renormalisation and factorisation scales by a factor of two changes the nominal signal cross section by 9–13% depending on the stop mass. The impact of detector-related uncertainties, such as JES, b-tagging and lepton ID efficiency, on the signal event yields varies between 10% and 25% and is dominated by the uncertainties on the JES.

8 Results and interpretation

The numbers of observed and expected SM background events in the two SRs are summarised in Table 1, for ee and $\mu\mu$ channels separately and summed. In all SRs, the expectation and observation agrees within uncertainties.

In Figure 3 the distributions of $E_{\mathrm{T}}^{\mathrm{miss}}$ in SR1, summing the ee and $\mu\mu$ channels, are shown. For illustrative purposes, the distributions expected for two signal ($\tilde{t}_1$,$\tilde{\chi}_1^0$) scenarios with masses of (250,100) GeV and (250,220) GeV, respectively, are added to the SM predictions. In Figures 4 and 5 the distributions of number of b-jets, p_{T} of leading and sub-leading jets are shown for events in SR1.

The results are translated into 95% confidence-level (C.L.) upper limits on contributions from new physics using the $\mathrm{CL_s}$ prescription [57]. The SR with the best expected sensitivity at each point in parameter space is adopted as the nominal result. Systematic uncertainties are treated as nuisance parameters and their correlations are taken into account. Figure 6 shows the observed and expected exclusion limits at 95% C.L. in the $\tilde{t}_1$-$\tilde{\chi}_1^0$ mass plane, assuming direct stop pair production in the framework of GMSB models with light higgsinos. The $\pm1\sigma$ contours around the median expected limit are also shown. Stop masses up to 310 GeV are excluded for 115 GeV $< m_{\tilde{\chi}_1^0} <$ 230 GeV. The exclusion extends to stop masses of 330 GeV for a neutralino mass of about 190 GeV. Stop masses below 240 GeV are excluded for all values of $\tilde{\chi}_1^0$ mass. The two SRs are used to set limits on the number of events and visible cross section, σ_{vis}, of new physics models not corrected for the effects of experimental acceptance and efficiency. The observed and expected excluded values at 95% C.L. are reported in Table 1.

	SR1	SR2
ee channel		
Data (2.05 fb^{-1})	39	20
SM	36.2±8.5	14.1±3.0
top	23.8±4.8	11.9±2.8
Z+hf	9.4±7.0	0.9±0.8
fake lepton	2.4±0.9	1.1±0.6
Others	0.5 ± 0.5	0.2 ± 0.2
$\mu\mu$ channel		
Data (2.05 fb^{-1})	47	23
SM	55 ± 12	26.6±5.1
top	40.4 ± 6.2	22.9 ± 4.3
Z+hf	14.2±9.9	3.3±2.6
fake lepton	0.00±0.08	0.00±0.07
Others	0.7 ± 0.7	0.3 ± 0.3
ee+$\mu\mu$		
Data (2.05 fb^{-1})	86	43
SM	92±19	40.7 ± 6.0
top	64.3±7.7	34.8 ± 5.0
Z+hf	24±16	4.2±3.2
fake lepton	2.4 ± 0.9	1.1 ± 0.6
Others	1.2 ± 1.2	0.6 ± 0.6

95% C.L. upper limits: observed (expected)		
events (2.05 fb^{-1})	37.2 (40.6)	19.8 (17.8)
visible σ [fb]	18.2 (19.8)	9.7 (8.7)

Table 1: Expected and measured number of events in SR1 and SR2 for *ee* and $\mu\mu$ channels (separately and summed) for an integrated luminosity of 2.05 fb^{-1}. The rows labelled as 'Others' report the sub-dominant SM backgrounds estimated from MC. The total systematic uncertainties are also displayed. Statistical uncertainties on the MC samples employed are negligible. In the bottom, model-independent observed and expected limits at 95% C.L on the number of events and visible cross sections are shown summing the *ee* and $\mu\mu$ channels.

9 Conclusions

In summary, results of a search for direct scalar top quark (stop) pair production in pp collisions at $\sqrt{s}$ = 7 TeV, based on 2.05 fb^{-1} of ATLAS data are reported. Stops are searched for in events with two same flavour opposite-sign leptons (e, μ) with invariant mass consistent with the Z boson mass, large missing transverse momentum and jets in the final state, where at least one of the jets is identified as originating from a b-quark. The results are in agreement with the SM prediction and are interpreted in the framework of R-parity conserving gauge-mediated-like 'natural' SUSY scenarios. Stop masses up to 310 GeV are excluded for 115 GeV $< m_{\tilde{\chi}_1^0} <$ 230 GeV at 95% C.L., reaching an exclusion of $m_{\tilde{t}_1} <$ 330 GeV for $m_{\tilde{\chi}_1^0} =$ 190 GeV.

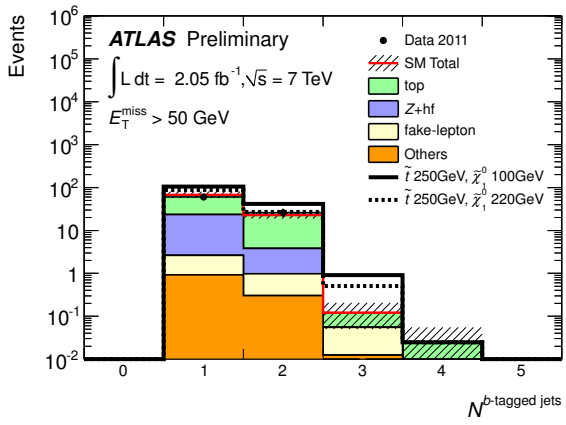

Figure 4: The distribution of the number of b-tagged jets for SR1 for the sum of ee and $\mu\mu$ channels. Data are compared to SM predictions (solid red line) and SM+signal predictions (solid and dashed black lines). The dashed grey band represents the experimental systematic uncertainties (JES, b-tagging efficiency).

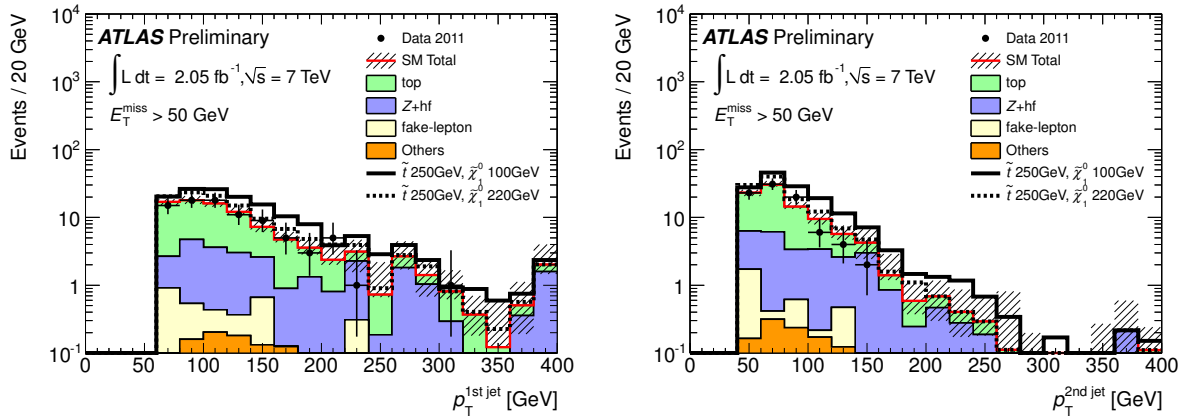

Figure 5: The distribution of the leading jet p_{T} (top) and the sub-leading jet p_{T} (bottom) for SR1 for the sum of ee and $\mu\mu$ channels. Data are compared to SM predictions (solid red line) and SM+signal predictions (solid and dashed black lines). The dashed grey band represents the sum of experimental systematic uncertainties (JES, b-tagging efficiency).

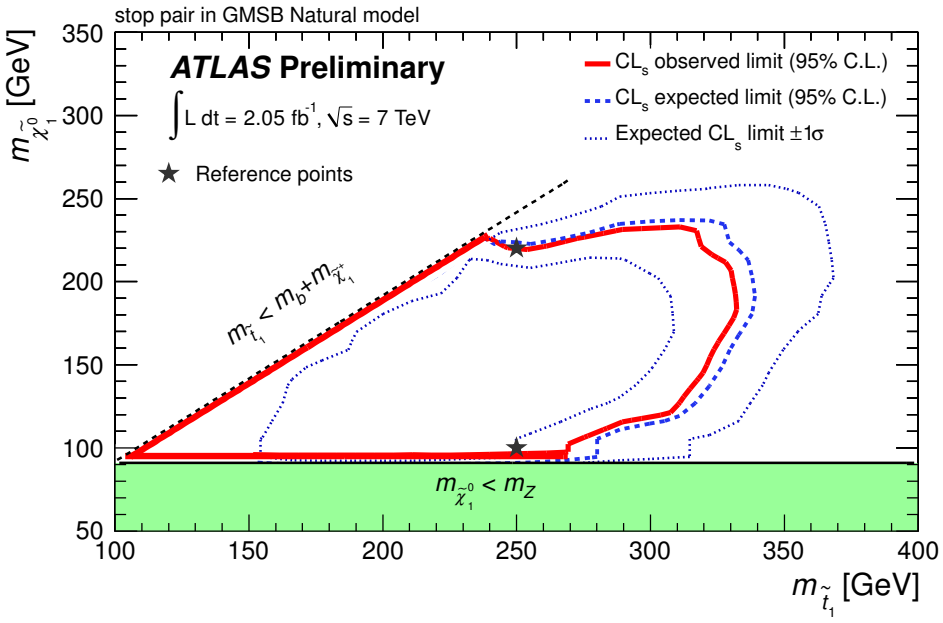

Figure 6: Expected and observed exclusion limits and $\pm 1\sigma$ variation on the expected limit in the $\tilde{t}_1$-$\tilde{\chi}_1^0$ mass plane. The reference points indicated on the plane correspond to the ($\tilde{t}_1$,$\tilde{\chi}_1^0$) scenarios of (250,100) GeV and (250,220) GeV, respectively.

References

[1] H. Miyazawa, *Baryon Number Changing Currents*, Prog. Theor. Phys. **36 (6)** (1966) 1266–1276.

[2] P. Ramond, *Dual Theory for Free Fermions*, Phys. Rev. **D3** (1971) 2415–2418.

[3] Y. A. Golfand and E. P. Likhtman, *Extension of the Algebra of Poincare Group Generators and Violation of p Invariance*, JETP Lett. **13** (1971) 323–326. [Pisma Zh.Eksp.Teor.Fiz.13:452-455,1971].

[4] A. Neveu and J. H. Schwarz, *Factorizable dual model of pions*, Nucl. Phys. **B31** (1971) 86–112.

[5] A. Neveu and J. H. Schwarz, *Quark Model of Dual Pions*, Phys. Rev. **D4** (1971) 1109–1111.

[6] J. Gervais and B. Sakita, *Field theory interpretation of supergauges in dual models*, Nucl. Phys. **B34** (1971) 632–639.

[7] D. V. Volkov and V. P. Akulov, *Is the Neutrino a Goldstone Particle?*, Phys. Lett. **B46** (1973) 109–110.

[8] J. Wess and B. Zumino, *A Lagrangian Model Invariant Under Supergauge Transformations*, Phys. Lett. **B49** (1974) 52.

[9] J. Wess and B. Zumino, *Supergauge Transformations in Four-Dimensions*, Nucl. Phys. **B70** (1974) 39–50.

[10] P. Fayet, *Supersymmetry and Weak, Electromagnetic and Strong Interactions*, Phys. Lett. **B64** (1976) 159.

[11] P. Fayet, *Spontaneously Broken Supersymmetric Theories of Weak, Electromagnetic and Strong Interactions*, Phys. Lett. **B69** (1977) 489.

[12] G. R. Farrar and P. Fayet, *Phenomenology of the Production, Decay, and Detection of New Hadronic States Associated with Supersymmetry*, Phys. Lett. **B76** (1978) 575–579.

[13] P. Fayet, *Relations Between the Masses of the Superpartners of Leptons and Quarks, the Goldstino Couplings and the Neutral Currents*, Phys. Lett. **B84** (1979) 416.

[14] S. Dimopoulos and H. Georgi, *Softly Broken Supersymmetry and SU(5)*, Nucl. Phys. **B193** (1981) 150.

[15] R. Kitano and Y. Nomura, *Supersymmetry, Natrualness, and Signatures at the LHC*, Phys. Rev. **D73** (2006) 095004.

[16] M. Dine and W. Fishler, *Phenomenological model of particle physics based on supersymmetry*, Phys. Lett. **B110** (1982) 227.

[17] M. Dine and A. E. Nelson, *Dynamical Supersymmetry Breaking at Low Energies*, Phys. Rev. **D48** (1993) 1277–1287.

[18] M. Asano, H. D. Kim, R. Kitano, and Y. Shimizu, *Natural Supersymmetry at the LHC*, JHEP **12** (2010) 019.

[19] ATLAS Collaboration, *Luminosity Determination in pp Collisions at sqrt(s)=7 TeV Using the ATLAS Detector at the LHC*, Eur. Phys. J. **C71** (2011) 1630.

[20] ATLAS Collaboration, *Luminosity Determination in pp Collisions at sqrt(s) = 7 TeV using the ATLAS Detector in 2011*, ATLAS-CONF-2011-116 (2011) .

[21] ATLAS Collaboration, *The ATLAS Experiment at the CERN Large Hadron Collider*, JINST **3** (2008) S08003.

[22] M. Bahr et al., *Herwig++ Physics and Manual*, Eur. Phys. J. **C58** (2008) 639–707.

[23] F. E. Paige et al., *ISAJET 7.69: A Monte Carlo event generator for pp, anti-p p, and e+e- reactions*, (2003) , arXiv:hep-ph/0312045.

[24] W. Beenakker et al., *Stop production at hadron colliders*, Nucl. Phys. **B515** (1998) 3–14.

[25] S. Moch and P. Uwer, *Heavy-quark pair production at two loops in QCD*, Nucl. Phys. Proc. Suppl. **183** (2008) 75–80.

[26] D. Stump et al., *Inclusive jet production, parton distributions, and the search for new physics*, JHEP **10** (2003) 046.

[27] A. Martin, W. Stirling, R. Thorne, and G. Watt, *Parton distributions for the LHC*, Eur.Phys.J. **C63** (2009) 189–285, 0901.0002.

[28] M. Botje, J. Butterworth, A. Cooper-Sarkar, A. de Roeck, J. Feltesse, et al., *The PDF4LHC Working Group Interim Recommendations*, arXiv:1101.0538 [hep-ph].

[29] S. Frixione and B. R. Webber, *The MC@NLO 3.2 Generator*, arXiv:0601192 [hep-ph].

[30] P. Nadolsky et al., *Implications of CTEQ global analysis for collider observables*, Phys. Rev. **D78** (2008) 013004.

[31] S. Frixione et al., *Matching NLO QCD computations with parton showers simulations: the POWHEG method*, JHEP **11** (2007) 070.

[32] B. Kersevan and E. Richter-Was, *The Monte Carlo event generator AcerMC version 2.0 with interfaces to PYTHIA 6.2 and HERWIG 6.5*, arXiv:hep-ph/0405247.

[33] M. Mangano et al., *ALPGEN, a generator for hard multiparton processes in hadronic collisions*, JHEP **07** (2003) 001.

[34] J. Pumplin et al., *New generation of parton distributions with uncertainties from global QCD analysis*, JHEP **07** (2002) 012.

[35] G. Corcella et al., *HERWIG 6: An event generator for hadron emission reactions with interfering gluons (including supersymmetric processes)*, JHEP **01** (2001) 010.

[36] J. M. Butterworth et al., *Multiparton interactions in photoproduction at HERA*, Z. Phys. **C72** (1996) 637–646.

[37] J. Alwall et al., *MadGraph 5 : Going Beyond*, JHEP **06** (2011) 128.

[38] T. Sjöstrand, S. Mrenna, and P. Skands, *PYTHIA 6.4 Physics and Manual*, JHEP **05** (2006) 026.

[39] ATLAS Collaboration, *Search for supersymmetry in pp collisions at $\sqrt{s} = 7$ TeV in final states with missing transverse momentum and b-jets with the ATLAS detector*, ATLAS-CONF-2012-003 (2012) .

[40] ATLAS Collaboration, *New ATLAS event generator tunes to 2010 data*, ATL-PHYS-PUB-2011-008 (2011) .

[41] ATLAS Collaboration, *The ATLAS Simulation Infrastructure*, Eur. Phys. J. **C70** (2010) 823–874.

[42] GEANT4 Collaboration, *GEANT4: A simulation toolkit*, Nucl. Instrum. Meth. **A506** (2003) 250–303.

[43] M. Cacciari and G. Salam, *Dispelling the N^3 myth for the k_t jet-finder*, Phys. Lett. **B641** (2006) 57–61.

[44] M. Cacciari et al., *The anti-k_t jet clustering algorithm*, JHEP **04** (2008) 063.

[45] W. Lampl et al., *Calorimeter Clustering Algorithms: Description and Performance*, ATL-LARG-PUB-2008-002 (2008) .

[46] ATLAS Collaboration, *Jet energy measurement with the ATLAS detector in proton-proton collisions at $\sqrt{s} = 7$ TeV*, submitted to Eur. Phys. J. C (2011) , `arXiv:1112.6426 [hep-ex]`.

[47] ATLAS Collaboration, *Commissioning of the ATLAS high-performance b-tagging algorithms in the 7 TeV collision data*, ATLAS-CONF-2011-102 (2011) .

[48] ATLAS Collaboration, *Electron performance measurements with the ATLAS detector using the 2010 LHC proton-proton collision data*, submitted to Eur. Phys. J. C (2011) , `arXiv:1110.3174 [hep-ex]`.

[49] ATLAS Collaboration, *Muon reconstruction efficiency in reporecessed 2010 LHC proton-proton collision data recorded with the ATLAS detector*, ATLAS-CONF-2011-063, 2011.

[50] ATLAS Collaboration, *Peformance of missing transverse momentum reconstruction in proton-proton collisions at 7 TeV with ATLAS*, Eur. Phys. J. **C72** (2012) 1844.

[51] ATLAS Collaboration, *A measurement of the ATLAS muon reconstruction and trigger efficiency using J/ψ decays*, ATLAS-CONF-2011-021 (2011) .

[52] ATLAS Collaboration, *Measurement of the top quark-pair production cross section with ATLAS in pp collisions at $\sqrt{s} = 7$ TeV*, Eur. Phys. J. **C71** (2011) 1577.

[53] ATLAS Collaboration, *Measurement of the Top Quark Pair Production Cross Section in pp Collisions at $\sqrt{s} = 7$ TeV in Dilepton Final States with ATLAS*, Phys. Lett. **B707** (2012) 459–477.

[54] ATLAS Collaboration, *Measurement of the cross-section for b-jets produced in association with a Z boson at $\sqrt{s} = 7$ TeV with the ATLAS detector*, Phys. Lett. **B706** (2012) 295–313.

[55] J. M. Compbell et al., *Associated Production of a Z Boson and a Single Heavy-Quark Jet*, Phys. Rev. **D69** (2004) 074021.

[56] J. Alwall et al., *Comparative study of various algorithms for the merging of parton showers and matrix elements in hadronic collisions*, Eur. Phys. J. **C53** (2008) 474–500.

[57] A. L. Read, *Presentation of search results : the CL_s technique*, J. Phys. G: Nucl. Part. Phys. **28** (2002) 2693.